

Modulating Bottom-Up and Top-Down Visual Processing via Language-Conditional Filters

İlker Keser, Ozan Arkan Can, Erkut Erdem, Aykut Erdem, Deniz Yuret

Abstract—How to best integrate linguistic and perceptual processing in multi-modal tasks that involve language and vision is an important open problem. In this work, we argue that the common practice of using language in a top-down manner, to direct visual attention over high-level visual features, may not be optimal. We hypothesize that the use of language to also condition the bottom-up processing from pixels to high-level features can provide benefits to the overall performance. To support our claim, we propose a model for language-vision problems involving dense prediction, and perform experiments on two different multi-modal tasks: image segmentation from referring expressions and language-guided image colorization. We compare results where either one or both of the top-down and bottom-up visual branches are conditioned on language. Our experiments reveal that using language to control the filters for bottom-up visual processing in addition to top-down attention leads to better results on both tasks and achieves state-of-the-art performance. Our analysis of different word types in input expressions suggest that the bottom-up conditioning is especially helpful in the presence of low level visual concepts like color.

Index Terms—Referring Expression Understanding, Segmentation from Referring Expressions, Colorization from Language, Language-Vision Problems, Grounded Language Understanding

I. INTRODUCTION

AS human beings, we can easily perceive our surroundings with our visual system and interact with each other using language. Since the work of Winograd et al. [1], developing a system that understands human language in a situated environment has been one of the long-standing goals of artificial intelligence. Recent successes of deep learning studies in both language and vision domains have increased the interest in tasks that combine language and vision [2]–[7]. However, how to best integrate linguistic and perceptual processing is still an important open problem. In this work, we investigate whether language should be used to control the filters for bottom-up visual processing as well as top-down attention.

In the human visual system, attention is driven by both *top-down* cognitive processes (e.g. focusing on a given shape or location) and *bottom-up* salient, behaviourally relevant

Manuscript submitted on 6 October, 2021. Currently under review for IEEE Transactions on Multimedia.

İlker Keser, Aykut Erdem, and Deniz Yuret are with KUIS AI Center, Koç University, Istanbul, Turkey (e-mail: ikesen16@ku.edu.tr; aerdem@ku.edu.tr; dyuret@ku.edu.tr).

Ozan Arkan Can contributed to this work prior to joining Amazon, as a part of Department of Computer Science and Engineering, Koç University, Istanbul, Turkey (e-mail: canozan@amazon.com).

Erkut Erdem is with Department of Computer Engineering, Hacettepe University, Ankara, Turkey (e-mail: erkut@hacettepe.edu.tr).

stimuli (e.g. fast moving objects and contrasting colors) [8]–[10]. Studies on embodied language explore the link between linguistic and perceptual representations [11]–[13] and often assume that language has a *high-level* effect on perception and drives the *top-down* visual attention [14]–[16]. However, recent studies from cognitive science point out that language comprehension also affects low-level visual processing [17]–[19]. Motivated by this, we propose a model¹ that can modulate either or both of *bottom-up* and *top-down* visual processing with language-conditional filters.

Current deep learning systems for language-vision tasks typically start with low-level image processing that is not conditioned on language, then connect the language representation with high level visual features to control the visual focus. To integrate both modalities, concatenation [20], element-wise multiplication [20]–[22] or attention from language to vision [3], [23]–[27] are commonly used. Specifically these studies do not condition low-level visual features on language. One exception is [28] which proposes conditioning the ResNet [29] image processing network with language conditioned batch normalization parameters at every stage. Our model differs from these architectures by having explicit *bottom-up* and *top-down* branches and allowing us to experiment with modulating one or both branches with language-conditional filters. Our proposed neural architecture is task agnostic and it can be used for integrated vision and language problems involving dense prediction.

The perceptual module of our model is based on the U-Net image segmentation architecture [30]. This architecture has clearly separated bottom-up and top-down branches which allows us to easily vary what parts are conditioned on language. The bottom-up branch starts from low level visual features and applies a sequence of contracting filters that result in successively higher level feature maps with lower spatial resolution. Following this is a top-down branch which takes the final low resolution feature map and applies a sequence of expanding filters that eventually result in a map with the original image resolution. Information flows between branches through skip connections between contracting and expanding filters at the same level. We experiment with conditioning one or both of these branches on language. We evaluate our model on two different language-vision tasks: image segmentation from referring expressions and language-guided image colorization.

In the *image segmentation from referring expressions* task,

¹We will release our code and pre-trained models along with a reproducible environment after the review process.

given an image and a natural language description, the aim is to obtain the segmentation mask that marks the object(s) described. We can contrast this with pure image based object detection [31], [32] and semantic segmentation [30], [33], [34] tasks which are limited to predefined semantic classes. The language input may contain various visual attributes (e.g., color, shape), spatial information (e.g., “on the right”, “in front of”), actions (e.g., “running”, “sitting”) and interactions/relations between different objects (e.g., “arm of the chair that the cat is sitting on”).

In *language-guided image colorization* task, given a grayscale image and a natural language description, the aim is to predict pixel color values. The absence of color information in the input images makes this problem interesting to experiment with because color words do not help in conditioning the bottom-up branch when the input consists of grayscale pixels.

To analyze our model in more detail, we focus on different subsets of examples based on words (e.g. adjectives, prepositions) and phrases (e.g. two consecutive nouns) included in the input expressions. We evaluate different configurations of our model on these subsets, where we modulate either one branch or both branches with language. On the subset where the input expressions include at least one color word, modulating only the bottom-up branch performs significantly better than modulating only the top-down branch in image segmentation. This suggests that conditioning the bottom-up branch on language is important when we have language that refers to low-level visual features. Our main model, which modulates both branches with language, improves both bottom-up and top-down baselines significantly, and achieves best results in all the subsets we have considered.

In the language-guided image colorization task, we find that when color information absent in input images, modulating only the bottom-up branch with language does not perform as well as the top-down baseline, and fails to predict and manipulate colors of target objects specified by input language. The top-down baseline can correctly color target objects, but it fails to apply the color to the whole surface, suggesting a segmentation problem. Our final model, which modulates both branches with language, improves both baselines by correctly coloring objects as a whole. This shows us that a language-conditional bottom-up visual branch still provides important complementary information to the model.

The rest of the paper is structured as follows: We summarize related work and compare it to our approach in Section II. We describe our model in detail in Section III. Our experimental results in Section IV show that modulating both top-down and bottom-up visual branches with language gives significant performance boost in two different language-vision problems involving dense prediction and give state-of-the-art results. Section V summarizes our contributions.

II. RELATED WORK

In this section, we briefly review prior work and tasks related to our study. We first examine referring expression comprehension and image segmentation from referring expressions, which aim at locating a bounding box or generating a segmentation mask for the object(s) described in the

language input, respectively. We then review language-guided image colorization where the goal is to predict colors for the monochromatic image under the guidance of textual input. Finally, we cover the works on language-conditional (dynamic) filters and studies that use them to modulate deep-learning models with language.

A. Referring Expression Comprehension

In referring expression comprehension problem, the goal is to locate a bounding box for the object(s) described in the input language. Early models for this task were typically built using a hybrid LSTM-CNN architecture [35], [36]. Most of the proposed solutions [37]–[40] rely on a region-based CNN (R-CNN) variant [32], [41], [42] to generate object proposals, and then assign scores to the object proposals depending on how much they match with input language. There are also numerous methods [37], [39], [43], [44] based on Neural Module Networks [45]. Apart from these methods, Multi-task Collaborative Network (MCN) [46] is trained jointly for referring expression comprehension and image segmentation from referring expression tasks. All these prior work condition only the top-down visual processing on language, where our proposed model conditions both visual processing branches on input language. Our model also does not depend on a pre-trained object detector.

B. Image Segmentation from Referring Expressions

In this task, the aim is to generate a segmentation mask for the object(s) referred in the input language [35]. To accomplish this task, multi-modal LSTM networks [47], [48], Convolutional LSTM (ConvLSTM) networks [47], [49]–[51], word-level attention mechanism [50]–[53], and cross-modal attention mechanism [54]–[56] have been used previously. Newer methods fuse language representation with multi-level visual representation [46], [57], [58]. Recently, Vision-Language Transformer (VLT) [59] has been emerged, which is a multi-modal encoder-decoder network based on transformers [60]. Like referring expression comprehension models, each one of the previous methods lacks a language-conditional bottom-up visual processing branch. Unlike these methods, Encoder Fusion Network (EFN) [61] conditions the bottom-up visual processing on input language, but it does not modulate the top-down branch with language. Our model has explicit language-conditional bottom-up and top-down visual branches, and our comprehensive experiments show that conditioning both branches on language boosts performance drastically by achieving state-of-the-art performance on several image segmentation from referring expressions benchmarks.

C. Language-guided Image Colorization

In language-guided image colorization task [62], the aim is to predict colors for all the pixels of a given input grayscale image based on text. This task bases its origins to image colorization task [63]–[66] which predicts the most probable colors solely based on visual input. Specifically, FiLMed ResNet [62] inserts extra Feature-wise Linear Modulation

(FiLM) layers [67] into a pre-trained ResNet-101 network [29] to predict color values in CIELAB color space. Multi-modal LSTMs [47], [68] and generative adversarial networks [69]–[71] are also used in this context to colorize sketch images. Among the literature, the most notable solution is Tag2Pix [72], which uses a U-Net-based image encoder to perform colorization on line art data for given input textual tags (e.g. black hair). Unlike our solution, Tag2Pix experiments on textual tags, not natural language and it does not modulate the condition through neither bottom-up nor top-down visual branches, which is the main contribution of our work.

D. Dynamic Filters

In this part, we review methods that use input-dependent dynamic filters/parameters to process visual features. To control a deep learning model with language, early work [28], [67] used conditional batch normalization layers with only language-conditioned coefficients rather than customized filters. Motion-Focused Predictive Models [73] generate action-conditioned dynamic filters. More recent methods [48], [74]–[78] generate language-conditioned dynamic filters to convolve visual features. Some image segmentation from referring expressions models [48], [77] also incorporate language-conditioned filters into the their architecture. LingUNet [78], which has an architecture similar to ours, adds language-conditioned filters to the top-down branch of U-Net to map instructions to actions in virtual environments. Unlike LingUNet, our architecture has also a language-conditioned visual processing branch which boosts performance dramatically. Each one of these methods uses language-conditioned parameters in either bottom-up visual branch [28], [67] or top-down visual branch [48], [77], [78]. Our comprehensive experiments on two different tasks show that modulating bottom-up branch with language is important to relate language to low-level visual cues.

III. THE MODEL

In this section, we describe our proposed model in detail. Fig. 1 shows an overview of our proposed architecture. First, the model extracts a tensor of low-level features using a pre-trained convolutional neural network and encodes the given natural language expression to a vector representation using a long short-term memory (LSTM) network [79]. Starting with the visual feature tensor, the model generates feature maps through a contracting and expanding path where the output head takes the final map and performs dense prediction, similar to U-Net [30]. Our proposed architecture modulates both of the the contracting and expanding paths with language using convolutional filters generated from the given expression which we refer to as *language-conditioned filters*. It is important to emphasize that the previous works either have a language-guided top-down or a language-conditioned bottom-up visual processing branch. As will be discussed in the next section, our experiments show that modulating both of these paths improves the performance dramatically by achieving the state-of-the art performance. In the following, we describe the details of each component of our model.

A. Low-level Image Features

Given an input image I , we extract visual features I_0 by using a pre-trained convolutional network. We use different pre-trained convolutional networks for different tasks to evaluate our approach fairly on both tasks, and share the entire configurations in Section IV-A1 and Section IV-B1. On the task of image segmentation from referring expressions, we concatenate 8-D location features to this feature map following the previous work [47], [50], [54], [80].

B. Language Representation

Consider a textual input $S = [w_1, w_2, \dots, w_n]$ where w_i represents the i 'th word. In this work, each word w_i is represented with a 300-dimensional GloVe embedding [81], i.e. $w_i \in \mathbb{R}^{300}$. We map the language input S to hidden states using a long short-term memory network [79] as $h_i = \text{LSTM}(h_{i-1}, w_i)$. We use the final hidden state of the LSTM as the textual representation, $r = h_n$. We set the size of hidden states to 256, i.e. $h_i \in \mathbb{R}^{256}$. Later on, we split this language representation into pieces to generate language-conditioned filters as explained in the next subsection.

C. Multi-modal Encoder

After generating image and language representations, our model generates a multi-modal feature map representing the input image and the given natural language expression. Our multi-modal encoder module extends U-Net [30] by conditioning both contracting and expanding branches on language using language-conditioned filters.

In the bottom-up branch, our model applies m convolutional modules to the image representation I_0 . Each module, CNN_i , takes the concatenation of the previously generated feature map (F_{i-1}) and its convolved version with language-conditioned filters K_i^F and produces an output feature map (F_i). Each CNN_i has a 2D convolution layer followed by batch normalization [82] and ReLU activation function [83]. The convolution layers have 5×5 filters with $stride = 2$ and $padding = 2$ halving the spatial resolution, and they all have the same number of output channels.

Similar to LingUNet [78], we split the textual representation r to m equal parts (t_i) to generate language kernels. We use each t_i to generate a language-conditioned filter for i th bottom-up layer (K_i^F):

$$K_i^F = \text{AFFINE}_i^F(\text{DROPOUT}(t_i)) \quad (1)$$

Each AFFINE_i^F is an affine transformation followed by normalizing and reshaping to convert the output to a convolutional filter. DROPOUT is the dropout regularization [84]. After obtaining the filter, we convolve it over the feature map obtained from the previous module (F_{i-1}) to relate expressions to image features:

$$G_i^F = \text{CONVOLVE}(K_i^F, F_{i-1}) \quad (2)$$

Then, the concatenation of these text-modulated features (G_i^F) for i th bottom-up layer and the previously generated features (F_{i-1}) is fed into module CNN_i for the next step.

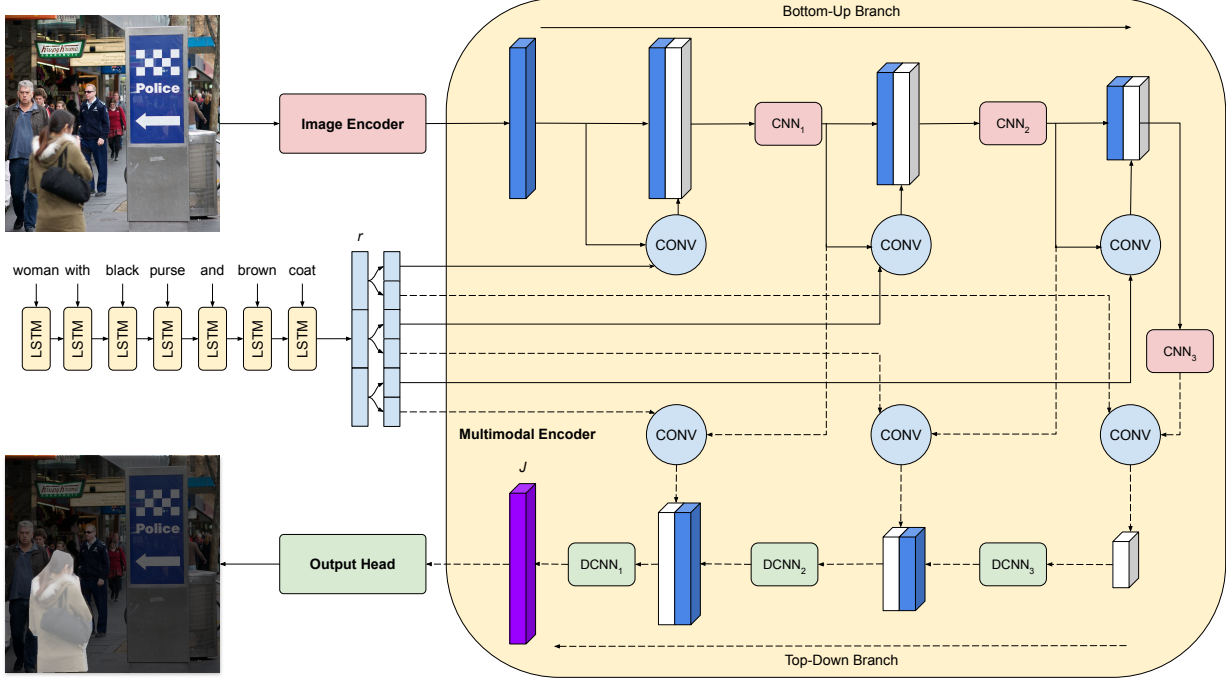


Fig. 1. Overview of the proposed model on the task of image segmentation from referring expressions. A pre-trained image encoder extracts low-level visual features. An LSTM network processes the input language, and then our model chops up the final hidden state r into pieces to generate language-conditional filters. Language-conditional filters and low-level visual features are fed into the multi-modal encoder. Each layer i of the bottom-up/contracting branch convolves the previous feature map F_{i-1} with language-conditional filters, concatenates output with previous feature map, and then a downsampling module CNN_i processes this concatenated feature map. Each layer i of the top-down/expanding branch convolves the bottom-up feature map obtained through the skip-connection, concatenates it with the previous top-down feature map H_{i+1} , and then an upsampling module DCNN_i processes this concatenated feature map. Finally, an output head takes the final feature map J , and performs dense prediction.

In the top-down branch, we generate m feature maps starting from the final output of the contracting branch as:

$$G_i^H = \text{CONVOLVE}(K_i^H, F_i) \quad (3)$$

$$H_m = \text{DCNN}_i(G_m^H) \quad (4)$$

$$H_i = \text{DCNN}_i(G_i^H \oplus H_{i-1}) \quad (5)$$

Similar to the bottom-up branch, G_i^H is the modulated feature map with language-conditional filters defined as:

$$K_i^H = \text{AFFINE}_i^H(\text{DROPOUT}(t_i)) \quad (6)$$

where AFFINE_i^H is again an affine transformation followed by normalizing and reshaping for i th layer of the top-down branch. Here, we convolve the filter (K_i^H) over the feature maps from the contracting branch (F_i). Each upsampling module DCNN_i gets the concatenation (\oplus) of the text related features and the feature map (H_i) generated from the previous module. Only the first module operates on just convolved features. Each DCNN_i consists of a 2D deconvolution layer followed by a batch normalization and ReLU activation function. The deconvolution layers have 5×5 filters with $stride = 2$ and $padding = 2$ doubling the spatial resolution, and they all have the same number of output channels. Final output H_1 becomes our joint feature map J representing the input image/natural language expression pair.

D. Output Heads

As mentioned earlier, we develop our model as a generic solution which can be used to solve language-vision problems involving dense prediction. In this direction, we adapt our model to two different tasks which are image segmentation from referring expressions and language-guided image colorization, to demonstrate the strength of our approach.

1) *Segmentation Head*: In the language-guided image segmentation problem, the goal is to generate segmentation mask for a given input image and language pair. After generating the joint feature map J , we apply a stack of layers (D_1, D_2, \dots, D_m) to map J to the exact image size. Similar to upsampling modules, each D_k is a 2D deconvolution layer followed by batch normalization and the ReLU activation. The deconvolutional layer has 5×5 filters with $stride = 2$ and $padding = 2$ to double the spatial sizes of the input. Each D_k preserves the number of channels except for the last one which maps the features to a single channel for the mask prediction. There is no batch norm operation and the ReLU activation for the final module, instead we apply a sigmoid function to turn the final features into probabilities ($P \in \mathbb{R}^{H \times W}$).

Given the probabilities ($P \in \mathbb{R}^{H \times W}$) for each pixel belonging to the target object(s), and the ground-truth mask $Y \in \mathbb{R}^{H \times W}$, the main training objective is the pixel-wise Binary-Cross-Entropy (BCE) loss:

$$\mathcal{L}_s = -\frac{1}{HW} \sum_i^H \sum_j^W Y_{ij} \log(P_{ij}) + (1 - Y_{ij}) \log(1 - P_{ij}) \quad (7)$$

2) *Colorization Head*: In language-guided colorization problem [62], the goal is to predict pixel color values for given input grayscale image with the guidance of input language. We worked with LAB color space by following the previous work on this task [62], [66]. We quantize a and b color values with bin size of 10, and use quantized a and b colors values as compound classes ab by following the prior work [66]. Our model predicts these compound ab classes. A convolutional layer with 3×3 filters generates class scores for each spatial location of joint language-image representation J . We perform bilinear upsampling to match input image size, and apply softmax operation to predict class probabilities for each pixel $P \in \mathbb{R}^{H \times W \times N}$ where N is the number of the ab classes.

Given the ab predicted probabilities for ab values P , and ground-truth color class indices $Y \in \mathbb{R}^{H \times W}$, we train our model by using weighted cross entropy loss objective,

$$\mathcal{L}_c = -\frac{1}{HWN} \sum_i^H \sum_j^W \sum_k^N W_k \{k = Y_{ij}\} \log(P_{ijk}) \quad (8)$$

Since the ab compound color class distribution is imbalanced, we use cross entropy loss with weights. We create the weight vector $W \in \mathbb{R}^N$ by following the exactly same process with the previous work [62], [66].

IV. EXPERIMENTS

In this section, we share the details of our experiments² on image segmentation from referring expressions (Section IV-A) and language-guided image colorization task (Section IV-B).

A. Image Segmentation from Referring Expressions

We first give the details of the datasets and our experimental configurations in Section IV-A1 for the image segmentation from referring expressions tasks. In Section IV-A2, we present our main results and compare our model with the state-of-the-art. Section IV-A3 shows some qualitative results. A detailed analysis of the contribution of our idea and the different parts of the architecture is given in Section IV-A4. Finally, in Section IV-A5 we divide a benchmark into subsets by categorizing input expressions, and evaluate different baselines on these subsets to analyze our approach in more detail.

1) Datasets and Experimental Setup:

Datasets: We evaluate our model on ReferIt (130.5k expressions, 19.9k images), UNC (142k expressions, 20k images), UNC+ (141.5k expressions, 20k images) [85] and Google-Ref (G-Ref) (104.5k expressions, 26.7k images) [36] [86] datasets. Unlike UNC, location-specific expressions are excluded in UNC+ through enforcing annotators to describe objects by their appearance. ReferIt, UNC, UNC+ datasets are collected through a two-player game [86] and have short expressions (avg. 4 words). G-Ref have longer and richer expressions, its expressions are collected from Amazon Mechanical Turk instead of a two-player game. G-Ref dataset has two different versions: (i) the original dataset [36] which includes two separate splits for training and validation, and (ii) the UMD

²We provide the implementation details, and present the complete ablation experiments and more qualitative examples in the supplementary material.

version [38] which includes three separate splits for training, validation, and testing. ReferIt images are collected from IAPR Tc-12 [87] and the others use images present in COCO [88].

Evaluation Metrics: Following the previous work [47], [48], [50], [54], we use intersection-over-union (IoU) and $pr@X$ as evaluation metrics. Given the predicted segmentation mask and the ground truth, the IoU metric is the ratio between the intersection and the union of the two. There are two different ways to calculate IoU : (i) the overall IoU calculates the total intersection over total union score throughout the entire dataset, and (i) the mean IoU calculates the mean of IoU scores of each individual example. For a fair comparison, we use both IoU metrics. The second metric, $pr@X$, calculates the percentage of the examples that have IoU score higher than the threshold X . In our experiments, $X \in \{0.5, 0.6, 0.7, 0.8, 0.9\}$.

2) *Quantitative Results*: Table I shows the comparison of our model with previous work. Bold faces highlight the highest achieved scores. “-” indicates that the model has not been evaluated on the dataset. Some of the recent models [46], [57]–[59] evaluate their models by using the mean IoU^3 metric instead of the overall IoU , and we denote these methods with †. To perform a fair evaluation with previous work, we evaluate our model by using both IoU metrics.

Table II presents the comparison of our model with the state-of-the-art in terms of $pr@X$ scores. The difference between our model and the state-of-the-art increases when the threshold increases. This indicates that our model is better at both finding and segmenting the referred objects including smaller ones.

3) *Qualitative Results*: We visualize some of the segmentation predictions of our model to gain better insights about the trained model. Fig. 2 shows some of the cases that our model segments correctly. These examples demonstrate that our model can learn a variety of language and visual reasoning patterns. For example, the first two examples of the fourth column show that our model learns to relate superlative adjectives (e.g., *taller*, *shorter*) with visual comparison. Examples including spatial prepositions (e.g., *on right*, *to the left of*, *near to*) demonstrate the spatial reasoning ability of the model. Our model can also learn a domain-specific nomenclature (e.g. *batter*, *catcher*) that is present in the dataset. Lastly, we can see that the model can also detect certain actions (e.g., *sitting*, *standing*).

4) *Ablation Study*: We implemented three different models, the top-down baseline, the bottom-up baseline, and our model, to show the effect of modulating language in expanding and contracting visual branches. While the bottom-up baseline modulates language in bottom-up branch only, the top-down baseline modulates language in top-down branch only. Our model conditions language on both branches. Table III shows us the results. The bottom-up baseline outperforms the top-down baseline with ≈ 2.7 IoU improvement. Modulating language in both visual branches yields the best results by improving the bottom-up baseline model with ≈ 2.85 IoU score.

³MCN, CGAN, and VLT uses the same open source implementation. Like these methods, LTS also has $pr@X$ scores significantly lower than our results, which indicates that they are also using the mean IoU , since it is directly proportional to the $pr@X$ metric.

TABLE I

COMPARISON WITH PREVIOUS WORK ON FOUR DATASETS. EVALUATION METRIC IS THE OVERALL *IoU* AND HIGHER IS BETTER. \dagger INDICATES THAT THE CORRESPONDING MODEL IS USING THE MEAN *IoU* FOR EVALUATION. *Backbone* DENOTES THE PRE-TRAINED IMAGE ENCODER USED. CHECK MARK \checkmark ON THE *DCRF* COLUMN INDICATES THAT THE CORRESPONDING METHOD USES THE DENSE CRF [89] POST-PROCESSING METHOD.

Method	Backbone	DCRF	UNC			UNC+			G-Ref			ReferIt
			val	testA	testB	val	testA	testB	val (G)	val (U)	test (U)	
CMSA [54]	ResNet-101	\checkmark	58.32	60.61	55.09	43.76	47.60	37.89	39.98	-	-	63.80
DC-LSTM [51]	ResNet-101	\checkmark	59.04	60.74	56.73	44.54	47.92	39.73	41.77	-	-	63.92
STEP [50]	ResNet-101	-	60.04	63.46	57.97	48.19	52.33	40.41	46.40	-	-	64.13
BRINet [55]	ResNet-101	\checkmark	61.35	63.37	59.57	48.57	52.87	42.13	48.04	-	-	63.46
CMPC [56]	ResNet-101	\checkmark	61.36	64.53	59.64	49.56	53.44	43.23	49.05	-	-	65.53
LSCM [53]	ResNet-101	\checkmark	61.47	64.99	59.55	49.34	53.12	43.50	48.05	-	-	66.57
EFN [61]	ResNet-101	-	62.76	65.69	59.67	51.50	55.24	43.01	51.93	-	-	66.70
BUSNet [90]	ResNet-101	\checkmark	63.27	66.41	61.39	51.76	56.87	44.13	50.56	-	-	-
Our model	ResNet-101	-	64.63	67.76	61.03	51.76	56.77	43.80	50.88	52.12	52.94	66.01
MCN \dagger [46]	DarkNet-53	-	62.44	64.20	59.71	50.62	54.99	44.69	-	49.22	49.40	-
CGAN \dagger [57]	DarkNet-53	-	64.86	68.04	62.07	51.03	55.51	44.06	46.54	51.01	51.69	-
LTS \dagger [58]	DarkNet-53	-	65.43	67.76	63.08	54.21	58.32	48.02	-	54.40	54.25	-
VLT \dagger [59]	DarkNet-53	-	65.65	68.29	62.73	55.50	59.20	49.36	49.76	52.99	56.65	-
Our model \dagger	ResNet-101	-	67.01	69.63	63.45	55.34	60.72	47.11	53.51	55.09	55.31	57.09



Fig. 2. Some correct predictions of our model on the UNC validation set. Each column shows various predictions for the same image.

Fig. 3 visualizes the predictions of the different models on the same examples. The bottom-up baseline performs better when the description has color information as we show in the first three examples. The top-down-only baseline also fails to detect object categories in some cases, and segments additional unwanted objects with similar category or appearance (e.g. *banana* vs. *orange*, and *mascot* vs. *player*). Overall, our model which conditions both visual branches on language gives the best results.

5) *Language-oriented Analysis*: To analyze the effect of language on model performance, we divided UNC testA/testB splits into subsets depending on the different types of words and phrases included in input expressions (e.g. color words, adverbs, adjectives, noun phrases with multiple adjectives). Table IV shows us the results of different models on these subsets. The first column stands for models, and the rest stand for different input expression categories. The notation of the categories are similar to Penn Treebank [91] Part of

TABLE II
COMPARISON WITH THE PREVIOUS WORKS ON THE VAL SET OF UNC DATASET WITH $pr@X$ METRICS.

Method	$pr@0.5$	$pr@0.6$	$pr@0.7$	$pr@0.8$	$pr@0.9$
CMSA [54]	66.44	59.70	50.77	35.52	10.96
DC-LSTM [51]	68.97	61.49	51.98	36.15	11.42
STEP [50]	70.15	63.37	53.15	36.53	10.45
BRINet [55]	71.83	65.05	55.64	39.36	11.21
LSCM [53]	70.84	63.82	53.67	38.69	12.06
EFN [61]	73.95	69.58	62.59	49.61	20.63
MCN [46]	76.60	70.33	58.39	33.68	5.26
LTS [58]	75.16	69.51	60.74	45.17	14.41
Our Model	76.67	71.77	64.76	51.69	22.73

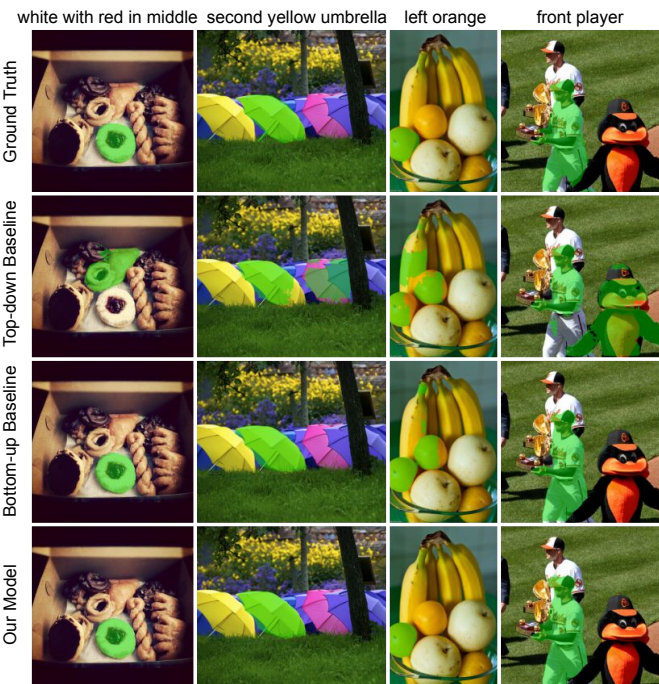


Fig. 3. Comparison of different architectural setups on the UNC test samples. Each column represents a different example. The first row stands for ground truth segmentation masks, and each of the remaining rows shows the results for the corresponding model.

Speech (POS) tags, where we denote prepositions with IN, examples with adjectives with JJ*, multiple adjectives with nJJ*, and colors with C. Preceding plus and minus signs stand for inclusion and exclusion. The number between parentheses shows us how many examples exist for the corresponding category. For instance, +IN,-C (3467) column stands for the subset with 3467 input expressions where each expression contains at least one preposition without any color words. Color words (e.g. red, light, darker, blue) has the most impact on the performance in comparison to other types of words and phrases. Our model and the bottom-up baseline performs significantly better than top-down baseline on the subset that includes colors. In the opposite case, where input expressions with colors are excluded, the top-down baseline has performance similar to the bottom-up baseline, and our final model

outperforms both single branch models. Since colors can be seen as low-level sensory information, low performance in the absence of the bottom-up branch can be expected. This gives us an example of the importance of conditioning the bottom-up visual branch on language to capture low-level visual concepts.

B. Language-guided Image Colorization

In this section we first give the details of the datasets and our experimental configurations (Section IV-B1) for the language-guided image colorization problem. Then, we present our quantitative results and compare our model with the previous work using various performance metrics in Section IV-B2. Finally, we share colorization outputs of different architectures to illustrate the effects of modulating language in either single branch or both branches (Section IV-B3).

1) Datasets and Experimental Setup:

Datasets: Following previous work [62], we use a modified version of COCO dataset [88] where the descriptions that do not contain color words are excluded. In this modified version, the training split has 66165, and the validation split has 32900 image / description pairs, and all images have a resolution of 224×224 pixels.

Evaluation Metrics: Following previous work [62], we use pixel-level top-1 (acc@1) and top-5 accuracies (acc@5) in LAB color space, and additionally peak signal-to-noise ratio (PSNR) in RGB color space to evaluate the performance of our model. In addition to those basic metrics, we also use Learned Perceptual Image Patch Similarity (LPIPS) [92] for further evaluation.

2) Quantitative Results: We present the quantitative performance of our model in Table V, and compare it with different design choices and previous work. A higher score is better for acc@1, acc@5 and PSNR metrics, and a lower score is better for LPIPS. FiLMed ResNet [62] uses FiLM [67] to perform language-conditional color prediction. FiLMed ResNet (ours) denotes the results reproduced by the implementation provided by the authors. To show the effect of language modulation on different branches, we train 3 different architectures: the top-down baseline, the bottom-up baseline and our model. While the top-down baseline modulates language only on the top-down visual branch, the bottom-up baseline modulates language on only the bottom-up visual branch, and our model performs language modulation on both branches. We also re-train our model by disabling class rebalancing and denote it as *Our Model wo/ balancing*.

Contrary to the segmentation experiments where the bottom-up baseline outperforms the top-down baseline on the subset which includes at least one color word per expression, the top-down baseline performs better than the bottom-up baseline on the colorization task in all performance measures. Since, color information is absent in input images, bottom-up visual branch cannot encode low-level image features by modulating color-dependent language. Nevertheless, the bottom-up baseline can help by predicting background objects like the sky and green fields (See Section IV-B3).

When we disable class rebalancing in the training phase, we observe a large performance increase in acc@1 and acc@5

TABLE III
ABLATION STUDY ON THE VALIDATION SET OF THE UNC DATASET WITH $pr@X$ AND OVERALL IoU METRICS.

Model	Backbone	$pr@0.5$	$pr@0.6$	$pr@0.7$	$pr@0.8$	$pr@0.9$	IoU
Top-down Baseline	ResNet-50	66.40	58.59	49.35	36.01	13.42	58.06
Bottom-up Baseline	ResNet-50	71.40	65.14	57.36	45.11	19.04	60.74
Our Model	ResNet-50	75.12	70.08	63.32	50.50	22.29	63.59
Our Model	ResNet-101	76.67	71.77	64.76	51.69	22.73	64.63

TABLE IV

PERFORMANCE ANALYSIS WITH IoU METRIC FOR DIFFERENT SETUPs DEPENDING ON THE INPUT EXPRESSION CATEGORIES FOR UNC TEST SPLITS.

Model	+C (2434)	-C (8318)	+IN (4702)	+IN,-C (3467)	+JJ* (5800)	+JJ*,-C (3505)	+n-JJ* (647)	+n-JJ*,-C (292)
Top-down Baseline	52.59	59.59	54.84	55.66	57.66	61.16	53.48	56.77
Bottom-up Baseline	60.40	60.02	56.05	55.49	61.18	61.86	55.55	53.96
Our Model	62.98	63.57	59.60	59.27	64.45	65.56	59.39	59.06

TABLE V

COLORIZATION RESULTS ON THE MODIFIED COCO VALIDATION SPLIT.

Method	acc@1	acc@5	PSNR	LPIPS
FiLMed ResNet [62]	23.70	60.50	-	-
FiLMed ResNet (ours) [62]	20.22	49.57	20.89	0.1280
Top-down Baseline	22.83	51.85	21.29	0.1226
Bottom-up Baseline	21.85	51.34	20.98	0.1448
Our Model	23.38	54.27	21.42	0.1262
Our Model w/o balancing	33.74	67.83	22.75	0.1250

accuracy metrics due to the imbalanced color distribution, where the model predicts the frequent colors exist in the backgrounds (e.g. **blue** in **sky** or **green** in **grass**).

3) *Qualitative Results*: We visualize some of the colorization predictions of our model to analyze them in more detail. Fig. 4 shows the color manipulation performance of the trained models. We experiment with different color conversions (e.g. from **red** to **blue** in second column). Each column represents an individual example. Each row shows the results for the corresponding model. FiLMed ResNet (ours) can understand all colorization hints, and it can manipulate object colors with some incorrectly predicted areas. The top-down baseline also performs similar to FiLMed ResNet (ours), where both baselines condition only the top-down visual branch on language.

In this task, since the models are blind to color, the bottom-up baseline loses its effectiveness to some degree, and starts to predict the most probable colors. This can be seen on the second and the last example, where the bottom-up baseline model predicts **red** for the stop sign and **blue** for the sky. Although, the bottom-up baseline performs worse in this task, modulating the bottom-up branch with language still contributes to our final model to localize and recognize the objects present in the scene. This can be seen on the third and the fifth examples, where the top-down baseline mixes colors up in some object parts (e.g. the red parts in the motorcycle and the blue parts in the sky). Our model w/o balancing tends to predict more grayish colors. This can be seen on the dog in the first example, the parts of the motorcycle in the third example, and the sky in the last example.

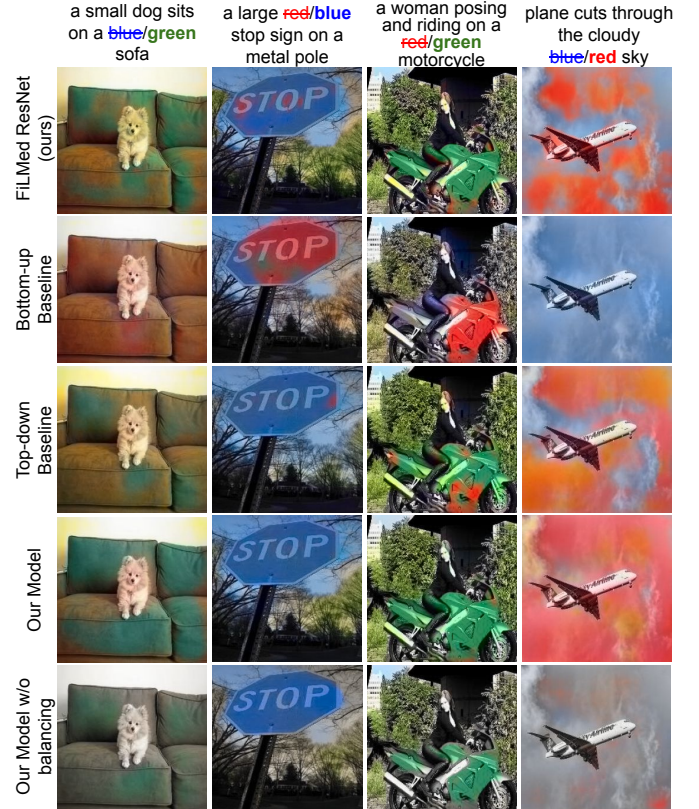


Fig. 4. Color manipulation performance of different models on COCO validation examples.

V. CONCLUSION

In this work, we suggested that conditioning both top-down and bottom-up visual branches on language is beneficial for grounding language to vision. To support our claim, we proposed a generic architecture for dense prediction problems involving language and vision, and performed experiments on two different language-vision tasks: image segmentation from referring expressions and language-guided image colorization. Our experiments on both tasks demonstrated that modulating both branches with language gives the best performance.

Our experiments on image segmentation from referring expressions task showed that modulating not only the top-down but also the bottom-up visual processing with language improves the performance significantly. Our proposed model achieves state-of-the-art results on 3 different segmentation benchmarks and performs significantly (≈ 5.5 and ≈ 2.9 IoU) better than its alternatives which condition only either the top-down branch, or the bottom-up branch on the input language.

To analyze our results further, we divided an image segmentation from referring expressions benchmark into subcategories depending on the types of words and phrases included in input language. Our experiments show that modulating the bottom-up branch with language gives a large performance improvement when color words are present in the input expressions, and modulating both branches with language gives the best results in all cases. This suggests that conditioning bottom-up visual branch on language is important especially when the expressions refer to low level visual features.

On the language-guided image colorization task, the bottom-up baseline failed to predict and manipulate colors of target objects effectively since the color information is absent in the input images. Nonetheless, a language-conditional bottom-up branch still helps our model identify the boundaries of the objects present in the grayscale input, and causes our combined model perform better than the top-down baseline in coloring whole objects.

ACKNOWLEDGEMENTS

This work was supported in part by an AI Fellowship to I. Kesenci provided by the Koç University Is Bank AI Center, GEBIP 2018 Award of the Turkish Academy of Sciences to E. Erdem, and BAGEP 2021 Award of the Science Academy to A. Erdem.

REFERENCES

- [1] T. Winograd, "Understanding natural language," *Cognitive psychology*, vol. 3, no. 1, pp. 1–191, 1972.
- [2] S. Antol, A. Agrawal, J. Lu, M. Mitchell, D. Batra, C. Lawrence Zitnick, and D. Parikh, "VQA: Visual Question Answering," in *ICCV*, Dec. 2015.
- [3] K. Xu, J. Ba, R. Kiros, K. Cho, A. Courville, R. Salakhudinov, R. Zemel, and Y. Bengio, "Show, attend and tell: Neural image caption generation with visual attention," in *ICML*, 2015, pp. 2048–2057.
- [4] R. Krishna, Y. Zhu, O. Groth, J. Johnson, K. Hata, J. Kravitz, S. Chen, Y. Kalantidis, L.-J. Li, D. A. Shamma *et al.*, "Visual genome: Connecting language and vision using crowdsourced dense image annotations," *IJCV*, vol. 123, no. 1, pp. 32–73, 2017.
- [5] A. Suhr, M. Lewis, J. Yeh, and Y. Artzi, "A Corpus of Natural Language for Visual Reasoning," in *ACL* vol. 2. Vancouver, Canada: Association for Computational Linguistics, Jul. 2017, pp. 217–223.
- [6] P. Anderson, Q. Wu, D. Teney, J. Bruce, M. Johnson, N. Sünderhauf, I. Reid, S. Gould, and A. van den Hengel, "Vision-and-Language Navigation: Interpreting Visually-Grounded Navigation Instructions in Real Environments," in *CVPR*, Jun. 2018.
- [7] D. A. Hudson and C. D. Manning, "GQA: A New Dataset for Real-World Visual Reasoning and Compositional Question Answering," *CVPR*, 2019.
- [8] M. Corbetta and G. L. Shulman, "Control of goal-directed and stimulus-driven attention in the brain," *Nature reviews neuroscience*, vol. 3, no. 3, pp. 201–215, 2002.
- [9] C. E. Connor, H. E. Egeth, and S. Yantis, "Visual attention: bottom-up versus top-down," *Current biology*, vol. 14, no. 19, pp. R850–R852, 2004.
- [10] J. Theeuwes, "Top-down and bottom-up control of visual selection," *Acta psychologica*, vol. 135, no. 2, pp. 77–99, 2010.
- [11] F. Pulvermüller, "Words in the brain's language," *Behavioral and brain sciences*, vol. 22, no. 2, pp. 253–279, 1999.
- [12] G. Vigliocco, D. P. Vinson, W. Lewis, and M. F. Garrett, "Representing the meanings of object and action words: The featural and unitary semantic space hypothesis," *Cognitive psychology*, vol. 48, no. 4, pp. 422–488, 2004.
- [13] V. Gallese and G. Lakoff, "The brain's concepts: The role of the sensory-motor system in conceptual knowledge," *Cognitive neuropsychology*, vol. 22, no. 3-4, pp. 455–479, 2005.
- [14] P. Bloom, *How children learn the meanings of words*. MIT press, 2002.
- [15] R. Jackendoff and R. S. Jackendoff, *Foundations of language: Brain, meaning, grammar, evolution*. Oxford University Press, USA, 2002.
- [16] B. Dessalegn and B. Landau, "More than meets the eye: The role of language in binding and maintaining feature conjunctions," *Psychological science*, vol. 19, no. 2, pp. 189–195, 2008.
- [17] L. Meteyard, B. Bahrami, and G. Vigliocco, "Motion detection and motion verbs: Language affects low-level visual perception," *Psychological Science*, vol. 18, no. 11, pp. 1007–1013, 2007.
- [18] B. Boutonnet and G. Lupyán, "Words jump-start vision: A label advantage in object recognition," *Journal of Neuroscience*, vol. 35, no. 25, pp. 9329–9335, 2015.
- [19] G. Lupyán and A. Clark, "Words and the world: Predictive coding and the language-perception-cognition interface," *Current Directions in Psychological Science*, vol. 24, no. 4, pp. 279–284, 2015, publisher: Sage Publications Sage CA: Los Angeles, CA.
- [20] M. Malinowski, M. Rohrbach, and M. Fritz, "Ask your neurons: A neural-based approach to answering questions about images," in *ICCV*, 2015, pp. 1–9.
- [21] J. Lu, J. Yang, D. Batra, and D. Parikh, "Hierarchical question-image co-attention for visual question answering," in *NeurIPS*, 2016, pp. 289–297.
- [22] J.-H. Kim, S.-W. Lee, D. Kwak, M.-O. Heo, J. Kim, J.-W. Ha, and B.-T. Zhang, "Multimodal residual learning for visual qa," in *NeurIPS*, 2016, pp. 361–369.
- [23] H. Xu and K. Saenko, "Ask, attend and answer: Exploring question-guided spatial attention for visual question answering," in *ECCV*. Springer, 2016, pp. 451–466.
- [24] Z. Yang, X. He, J. Gao, L. Deng, and A. Smola, "Stacked Attention Networks for Image Question Answering," in *CVPR*, Jun. 2016.
- [25] J. Lu, C. Xiong, D. Parikh, and R. Socher, "Knowing when to look: Adaptive attention via a visual sentinel for image captioning," in *CVPR*, 2017, pp. 375–383.
- [26] P. Anderson, X. He, C. Buehler, D. Teney, M. Johnson, S. Gould, and L. Zhang, "Bottom-up and top-down attention for image captioning and visual question answering," in *CVPR*, 2018, pp. 6077–6086.
- [27] R. Zellers, Y. Bisk, A. Farhadi, and Y. Choi, "From Recognition to Cognition: Visual Commonsense Reasoning," in *CVPR*, Jun. 2019.
- [28] H. De Vries, F. Strub, J. Mary, H. Larochelle, O. Pietquin, and A. C. Courville, "Modulating early visual processing by language," in *NeurIPS*, 2017, pp. 6594–6604.
- [29] K. He, X. Zhang, S. Ren, and J. Sun, "Deep residual learning for image recognition," in *CVPR*, 2016, pp. 770–778.
- [30] O. Ronneberger, P. Fischer, and T. Brox, "U-net: Convolutional networks for biomedical image segmentation," in *MICCAI*, 2015, pp. 234–241.
- [31] R. Girshick, "Fast R-CNN" *ICCV*, Dec. 2015.
- [32] S. Ren, K. He, R. Girshick, and J. Sun, "Faster R-CNN: Towards Real-Time Object Detection with Region Proposal Networks," *TPAMI*, vol. 39, no. 6, pp. 1137–1149, Jun. 2017.
- [33] J. Long, E. Shelhamer, and T. Darrell, "Fully convolutional networks for semantic segmentation," in *CVPR*, 2015, pp. 3431–3440.
- [34] L.-C. Chen, G. Papandreou, I. Kokkinos, K. Murphy, and A. L. Yuille, "Deeplab: Semantic image segmentation with deep convolutional nets, atrous convolution, and fully connected crfs," *TPAMI*, vol. 40, no. 4, pp. 834–848, 2017.
- [35] R. Hu, M. Rohrbach, and T. Darrell, "Segmentation from Natural Language Expressions," *Lecture Notes in Computer Science*, pp. 108–124, 2016.
- [36] J. Mao, J. Huang, A. Toshev, O. Camburu, A. Yuille, and K. Murphy, "Generation and Comprehension of Unambiguous Object Descriptions," *CVPR*, Jun. 2016.
- [37] R. Hu, M. Rohrbach, J. Andreas, T. Darrell, and K. Saenko, "Modeling Relationships in Referential Expressions with Compositional Modular Networks," *CVPR*, Jul. 2017.
- [38] V. K. Nagaraja, V. I. Morariu, and L. S. Davis, "Modeling Context Between Objects for Referring Expression Understanding," *Lecture Notes in Computer Science*, pp. 792–807, 2016.

[39] L. Yu, Z. Lin, X. Shen, J. Yang, X. Lu, M. Bansal, and T. L. Berg, “MAttNet: Modular Attention Network for Referring Expression Comprehension,” *CVPR*, Jun. 2018.

[40] P. Wang, Q. Wu, J. Cao, C. Shen, L. Gao, and A. v. d. Hengel, “Neighbourhood Watch: Referring Expression Comprehension via Language-Guided Graph Attention Networks,” *CVPR*, Jun. 2019.

[41] R. Girshick, J. Donahue, T. Darrell, and J. Malik, “Rich Feature Hierarchies for Accurate Object Detection and Semantic Segmentation,” *CVPR*, Jun. 2014.

[42] K. He, G. Gkioxari, P. Dollar, and R. Girshick, “Mask R-CNN,” *ICCV*, Oct. 2017.

[43] V. Cirik, T. Berg-Kirkpatrick, and L.-P. Morency, “Using syntax to ground referring expressions in natural images,” in *AAAI*, 2018.

[44] D. Liu, H. Zhang, F. Wu, and Z.-J. Zha, “Learning to Assemble Neural Module Tree Networks for Visual Grounding,” in *ICCV*, Oct. 2019.

[45] J. Andreas, M. Rohrbach, T. Darrell, and D. Klein, “Neural module networks,” in *CVPR*, 2016, pp. 39–48.

[46] G. Luo, Y. Zhou, X. Sun, L. Cao, C. Wu, C. Deng, and R. Ji, “Multi-task collaborative network for joint referring expression comprehension and segmentation,” in *CVPR*, 2020, pp. 10 034–10 043.

[47] C. Liu, Z. L. Lin, X. Shen, J. Yang, X. Lu, and A. L. Yuille, “Recurrent Multimodal Interaction for Referring Image Segmentation,” *ICCV*, pp. 1280–1289, 2017.

[48] E. Margffoy-Tuay, J. C. Pérez, E. Botero, and P. Arbeláez, “Dynamic multimodal instance segmentation guided by natural language queries,” in *ECCV*, 2018, pp. 630–645.

[49] X. Shi, Z. Chen, H. Wang, D.-Y. Yeung, W.-k. Wong, and W.-c. WOO, “Convolutional LSTM Network: A Machine Learning Approach for Precipitation Nowcasting,” in *NeurIPS*, 2015, pp. 802–810.

[50] D.-J. Chen, S. Jia, Y.-C. Lo, H.-T. Chen, and T.-L. Liu, “See-through-text grouping for referring image segmentation,” in *ICCV*, 2019, pp. 7454–7463.

[51] L. Ye, Z. Liu, and Y. Wang, “Dual convolutional lstm network for referring image segmentation,” *TMM*, vol. 22, no. 12, pp. 3224–3235, 2020.

[52] H. Shi, H. Li, F. Meng, and Q. Wu, “Key-Word-Aware Network for Referring Expression Image Segmentation,” in *ECCV*, Sep. 2018.

[53] T. Hui, S. Liu, S. Huang, G. Li, S. Yu, F. Zhang, and J. Han, “Linguistic structure guided context modeling for referring image segmentation,” in *ECCV*. Springer, 2020, pp. 59–75.

[54] L. Ye, M. Rochan, Z. Liu, and Y. Wang, “Cross-Modal Self-Attention Network for Referring Image Segmentation,” *CVPR*, Jun. 2019.

[55] Z. Hu, G. Feng, J. Sun, L. Zhang, and H. Lu, “Bi-Directional Relationship Inferring Network for Referring Image Segmentation,” in *CVPR*, 2020, pp. 4424–4433.

[56] S. Huang, T. Hui, S. Liu, G. Li, Y. Wei, J. Han, L. Liu, and B. Li, “Referring image segmentation via cross-modal progressive comprehension,” in *CVPR*, 2020, pp. 10 488–10 497.

[57] G. Luo, Y. Zhou, R. Ji, X. Sun, J. Su, C.-W. Lin, and Q. Tian, “Cascade grouped attention network for referring expression segmentation,” in *Proceedings of the 28th ACM International Conference on Multimedia*, 2020, pp. 1274–1282.

[58] Y. Jing, T. Kong, W. Wang, L. Wang, L. Li, and T. Tan, “Locate then segment: A strong pipeline for referring image segmentation,” in *CVPR*, 2021, pp. 9858–9867.

[59] H. Ding, C. Liu, S. Wang, and X. Jiang, “Vision-language transformer and query generation for referring segmentation,” in *ICCV*, 2021.

[60] A. Vaswani, N. Shazeer, N. Parmar, J. Uszkoreit, L. Jones, A. N. Gomez, Ł. Kaiser, and I. Polosukhin, “Attention is all you need,” in *NeurIPS*, 2017, pp. 5998–6008.

[61] G. Feng, Z. Hu, L. Zhang, and H. Lu, “Encoder fusion network with co-attention embedding for referring image segmentation,” in *CVPR*, 2021, pp. 15 506–15 515.

[62] V. Manjunatha, M. Iyyer, J. Boyd-Graber, and L. Davis, “Learning to color from language,” in *NAACL-HLT*, vol. 2, Jun. 2018, pp. 764–769.

[63] Z. Cheng, Q. Yang, and B. Sheng, “Deep colorization,” in *ICCV*, 2015, pp. 415–423.

[64] S. Iizuka, E. Simo-Serra, and H. Ishikawa, “Let there be color! Joint end-to-end learning of global and local image priors for automatic image colorization with simultaneous classification,” *ToG*, vol. 35, no. 4, pp. 1–11, 2016.

[65] G. Larsson, M. Maire, and G. Shakhnarovich, “Learning representations for automatic colorization,” in *ECCV*. Springer, 2016, pp. 577–593.

[66] R. Zhang, P. Isola, and A. A. Efros, “Colorful image colorization,” in *ECCV*, 2016, pp. 649–666.

[67] E. Perez, F. Strub, H. d. Vries, V. Dumoulin, and A. C. Courville, “FiLM: Visual Reasoning with a General Conditioning Layer,” in *AAAI*, 2018.

[68] C. Zou, H. Mo, C. Gao, R. Du, and H. Fu, “Language-based colorization of scene sketches,” *TOG*, vol. 38, no. 6, pp. 1–16, 2019, publisher: ACM New York, NY, USA.

[69] I. Goodfellow, J. Pouget-Abadie, M. Mirza, B. Xu, D. Warde-Farley, S. Ozair, A. Courville, and Y. Bengio, “Generative adversarial nets,” in *NeurIPS*, Z. Ghahramani, M. Welling, C. Cortes, N. Lawrence, and K. Q. Weinberger, Eds., vol. 27, 2014.

[70] H. Bahng, S. Yoo, W. Cho, D. K. Park, Z. Wu, X. Ma, and J. Choo, “Coloring with words: Guiding image colorization through text-based palette generation,” in *ECCV*, 2018, pp. 431–447.

[71] J. Chen, Y. Shen, J. Gao, J. Liu, and X. Liu, “Language-based image editing with recurrent attentive models,” in *CVPR*, 2018, pp. 8721–8729.

[72] H. Kim, H. Y. Jhoo, E. Park, and S. Yoo, “Tag2pix: Line art colorization using text tag with secat and changing loss,” in *ICCV*, 2019, pp. 9056–9065.

[73] C. Finn, I. Goodfellow, and S. Levine, “Unsupervised learning for physical interaction through video prediction,” in *NeurIPS*, 2016, pp. 64–72.

[74] Z. Li, R. Tao, E. Gavves, C. G. Snoek, and A. W. Smeulders, “Tracking by natural language specification,” in *CVPR*, 2017, pp. 6495–6503.

[75] P. Gao, H. Li, S. Li, P. Lu, Y. Li, S. C. Hoi, and X. Wang, “Question-guided hybrid convolution for visual question answering,” in *ECCV*, 2018, pp. 469–485.

[76] K. Gavrilyuk, A. Ghodrati, Z. Li, and C. G. Snoek, “Actor and action video segmentation from a sentence,” in *CVPR*, 2018, pp. 5958–5966.

[77] Y.-W. Chen, Y.-H. Tsai, T. Wang, Y.-Y. Lin, and M.-H. Yang, “Referring Expression Object Segmentation with Caption-Aware Consistency,” in *BMVC*, 2019.

[78] D. Misra, A. Bennett, V. Blukis, E. Niklasson, M. Shatkhin, and Y. Artzi, “Mapping instructions to actions in 3D environments with visual goal prediction,” in *EMNLP*, Oct.-Nov. 2018, pp. 2667–2678.

[79] S. Hochreiter and J. Schmidhuber, “Long short-term memory,” *Neural computation*, vol. 9, no. 8, pp. 1735–1780, 1997.

[80] R. Hu, H. Xu, M. Rohrbach, J. Feng, K. Saenko, and T. Darrell, “Natural Language Object Retrieval,” *CVPR*, Jun. 2016.

[81] J. Pennington, R. Socher, and C. D. Manning, “Glove: Global vectors for word representation,” in *EMNLP*, 2014, pp. 1532–1543.

[82] S. Ioffe and C. Szegedy, “Batch normalization: Accelerating deep network training by reducing internal covariate shift,” in *ICML*. PMLR, 2015, pp. 448–456.

[83] A. L. Maas, A. Y. Hannun, and A. Y. Ng, “Rectifier nonlinearities improve neural network acoustic models,” in *ICML*, vol. 30, 2013, p. 3.

[84] N. Srivastava, G. Hinton, A. Krizhevsky, I. Sutskever, and R. Salakhutdinov, “Dropout: a simple way to prevent neural networks from overfitting,” *JMLR*, vol. 15, no. 1, pp. 1929–1958, 2014.

[85] L. Yu, P. Poirson, S. Yang, A. C. Berg, and T. L. Berg, “Modeling Context in Referring Expressions,” *Lecture Notes in Computer Science*, pp. 69–85, 2016.

[86] S. Kazemzadeh, V. Ordonez, M. Matten, and T. Berg, “Referitgame: Referring to objects in photographs of natural scenes,” in *EMNLP*, 2014, pp. 787–798.

[87] H. J. Escalante, C. A. Hernández, J. A. Gonzalez, A. López-López, M. Montes, E. F. Morales, L. E. Sucar, L. Villaseñor, and M. Grubinger, “The segmented and annotated IAPR TC-12 benchmark,” *Computer vision and image understanding*, vol. 114, no. 4, pp. 419–428, 2010.

[88] T.-Y. Lin, M. Maire, S. Belongie, J. Hays, P. Perona, D. Ramanan, P. Dollár, and C. L. Zitnick, “Microsoft coco: Common objects in context,” in *ECCV*, 2014, pp. 740–755.

[89] P. Krähenbühl and V. Koltun, “Efficient inference in fully connected crfs with gaussian edge potentials,” *NeurIPS*, vol. 24, pp. 109–117, 2011.

[90] S. Yang, M. Xia, G. Li, H.-Y. Zhou, and Y. Yu, “Bottom-up shift and reasoning for referring image segmentation,” in *CVPR*, 2021, pp. 11 266–11 275.

[91] M. P. Marcus, M. A. Marcinkiewicz, and B. Santorini, “Building a large annotated corpus of english: the penn treebank,” *Computational Linguistics*, vol. 19, no. 2, pp. 313–330, 1993.

[92] R. Zhang, P. Isola, A. A. Efros, E. Shechtman, and O. Wang, “The unreasonable effectiveness of deep features as a perceptual metric,” in *CVPR*, 2018.

[93] D. P. Kingma and J. Ba, “Adam: A method for stochastic optimization,” *arXiv preprint arXiv:1412.6980*, 2014.

[94] J. Devlin, M.-W. Chang, K. Lee, and K. Toutanova, “BERT: Pre-training of deep bidirectional transformers for language understanding,” in *ACL*, Jun. 2019, pp. 4171–4186.

SUPPLEMENTARY MATERIAL

This supplementary material contains the implementation details (Section A), the complete ablation studies (Section B), and more qualitative results (Section C) of our work, *Modulating Bottom-Up and Top-Down Visual Processing via Language-Conditional Filters*.

A. Implementation Details

In this part, we share the detailed configurations of our model on *image segmentation from referring expressions* and *language-guided image colorization* tasks.

1) *Image Segmentation from Referring Expressions*: Following previous work [47], [48], [50], [54], we limit the maximum length of expressions to 20. We set input image size to 512×512 and 640×640 for training and inference phase respectively. We use the first four layers of DeepLabv3+ with ResNet-101 backbone, pre-trained on COCO dataset by excluding images appear on the validation and the test sets of UNC, UNC+ and G-Ref datasets similar to previous work [39], [46], [59]. Thus, our low-level visual feature map I has the size of $64 \times 64 \times 64 \times 1032$ in training, and $80 \times 80 \times 1032$ in inference phase, both including 8-D location features. In all convolutional layers, we set the filter size, stride, and number of filters (ch) as $(5, 5)$, 2, and 512, respectively. The depth is 4 in the multimodal encoder part of the network. We set the dropout probability to 0.2 throughout the network. We use Adam optimizer [93] with default parameters. We freeze the DeepLab-v3+ ResNet-101 weights. There are 32 examples in each minibatch. We train our model for 20 epochs on a Tesla V100 GPU with mixed precision and each epoch takes at most two hours depending on the dataset.

2) *Language-guided Image Colorization*: For all the convolutional layers in the multimodal encoder, we set the filter size and stride as $(5, 5)$ and 2. Like our segmentation network, the multimodal encoder of our colorization model has a depth of 4. We apply dropout with 0.2 probability throughout the network. We set the number of language-conditional filters as 512, replace the LSTM encoder with a BiLSTM encoder, and we use the first two layers of ResNet-101 trained on ImageNet as image encoder to have a similar model capacity and make a fair comparison with the previous work [62]. We set input image width and height to 224 in both training and validation. Thus, the low-level visual feature map has the size of $28 \times 28 \times 512$, and we don't use location features. Additionally, in our experimental analysis, we consider the same design choices with previous work [62], [66]. Specifically, we use LAB color space, and our model predicts ab color values for all the pixels of the input image. We perform the class rebalancing procedure to obtain class weights for weighted cross entropy objective. We use 313 ab classes present in ImageNet dataset, and encode ab color values to classes by assigning them to their nearest neighbors. We use input images with a size of 224×224 , and output target images with a size of 56×56 which is same with the previous work.

B. Ablation Studies

We performed additional ablation experiments on *image segmentation from referring expressions* task in order to un-

derstand the contributions of the remaining components of our model. We share results in Table SI. Each row stands for a different architectural setup. Horizontal lines separate the different ablation studies we performed, and first column denotes the ablation study group. Columns on the left determine these architectural setups. \checkmark on the *Top-down* column indicates that the corresponding setup modulates top-down visual branch with language, and similarly \checkmark on the *Bottom-up* column indicates that the corresponding setup modulates bottom-up visual branch with language. *Depth* indicates how many layers the multi-modal encoder has. *Layer* indicates the type of language-conditional layer used. *Visual* and *Textual* indicates which visual encoder and textual encoder used for the corresponding setup, respectively. The remaining columns stand for results.

Network Depth (2): We performed experiments by varying the depth size of the multi-modal encoder. We originally started with the depth size of 4. Increasing the depth size slightly increased the scores for some metrics, but more importantly, decreasing the depth size caused the model to perform worse than the bottom-up baseline. This happens because decreasing the depth size shrinks the receptive field of the network, and the model becomes less capable of drawing conclusions for the scenes that requires to be seen as a whole in order to fully understand.

FiLM layers vs. Language-conditional Filters (3): Another method for modulating language is using conditional batch normalization [28] or its successor, FiLM layers. When we replaced language-conditional filters with FiLM layers in our model, we observed ≈ 2.5 IoU decrease. This is natural, since the FiLM layer can be thought as grouped convolution with language-conditional filters, where the number of groups is equal to number of channels / filters.

LSTM vs. BERT as language encoder (4): We also experimented with BERT [94] as input language encoder in addition to LSTM network. We update BERT weights simultaneously with the rest of our model, where we use a smaller learning rate for BERT (0.00005). We use the *CLS* output embedding as our language representation r , than split this embedding into pieces to create language-conditional filters. Our model achieved similar quantitative results using BERT as language encoder. This points out a language encoder pre-trained on solely textual data might be sub-optimal and unnecessary for integrating vision and language.

The impact of the visual backbone (5): We first start training our model with DeepLabv3+ ResNet-50 backbone pre-trained on Pascal VOC dataset. Then, we pre-trained a DeepLabv3+ with ResNet-101 backbone on COCO dataset by excluding the images appear on the validation and the test splits of all benchmarks similar to the previous work [39], [46], [59]. We only used 20 object categories present in Pascal VOC dataset. Thus, using a more sophisticated visual backbone resulted with ≈ 1 improvement on the overall *IoU* score.

C. Qualitative Results

In this part, we share more qualitative results produced by our proposed model.

TABLE SI
THE COMPLETE ABLATION STUDIES ON THE VALIDATION SET OF THE UNC DATASET WITH $pr@X$ AND OVERALL IoU METRICS.

#	Top-down	Bottom-up	Depth	Layer	Visual	Textual	$pr@0.5$	$pr@0.6$	$pr@0.7$	$pr@0.8$	$pr@0.9$	IoU
1	✓		4	Conv	ResNet-50	LSTM	66.40	58.59	49.35	36.01	13.42	58.06
		✓	4	Conv	ResNet-50	LSTM	71.40	65.14	57.36	45.11	19.04	60.74
	✓	✓	4	Conv	ResNet-50	LSTM	75.12	70.08	63.32	50.50	22.29	63.59
2	✓	✓	3	Conv	ResNet-50	LSTM	69.96	63.13	55.04	41.33	15.98	60.23
	✓	✓	4	Conv	ResNet-50	LSTM	75.12	70.08	63.32	50.50	22.29	63.59
	✓	✓	5	Conv	ResNet-50	LSTM	75.56	70.59	63.82	51.68	22.84	63.52
3	✓	✓	4	Conv	ResNet-50	LSTM	75.12	70.08	63.32	50.50	22.29	63.59
	✓	✓	4	FiLM	ResNet-50	LSTM	71.18	65.14	57.32	44.66	18.75	61.12
4	✓	✓	4	Conv	ResNet-50	LSTM	75.12	70.08	63.32	50.50	22.29	63.59
	✓	✓	4	Conv	ResNet-50	BERT	75.60	70.39	63.05	49.93	21.16	63.57
5	✓	✓	4	Conv	ResNet-50	LSTM	75.12	70.08	63.32	50.50	22.29	63.59
	✓	✓	4	Conv	ResNet-101	LSTM	76.67	71.77	64.76	51.69	22.73	64.63

D. Image Segmentation from Referring Expressions

Fig. S1 shows some of the incorrect segmentation predictions from our model on the UNC test split. Examples in (a) show that our model tends to fail in case of typos. Our model segments the correct objects for these two examples when the typos are fixed (e.g. *pink* instead of *pick*). Examples in (b) show that some of the expressions are ambiguous, where there are multiple objects that could be referred to by the expression. In this case, the model seems to segment the most salient object. Some of the annotations contain incorrect or incomplete ground-truth mask (c). Finally, some of the examples (d) are hard to segment completely due to the lack of light or objects that mask the referred objects.

1) Language-guided Image Colorization:

In Fig. S2, we share some successful and some unsuccessful visual results produced by our model. We present general success cases with the first four examples on the left side of Fig. S2. The first and the second examples show that our model is capable of localizing, detecting and colorizing large objects present in the input image. In the third example, we share results for a black and white image. In the dataset, $\approx 3\%$ of images are grayscale images, and our model performs well in these examples. Finally, the last successful example shows that our model performs well on colorizing common background objects like sky and grass. The right side of Fig. S2 highlights some of the failure cases we observed throughout the dataset. In the first two examples, our model is able to localize and recognize the target objects, but it fails to colorize them successfully by colorizing not only the targeted parts but also other parts. Models generally fail to colorize small objects since the data is imbalanced and it contains vast backgrounds and big objects frequently. The last two examples show that models fail to colorize reflective or transparent objects like glasses or water, these were also difficult in the language based segmentation task (see Fig. S1 (d)).

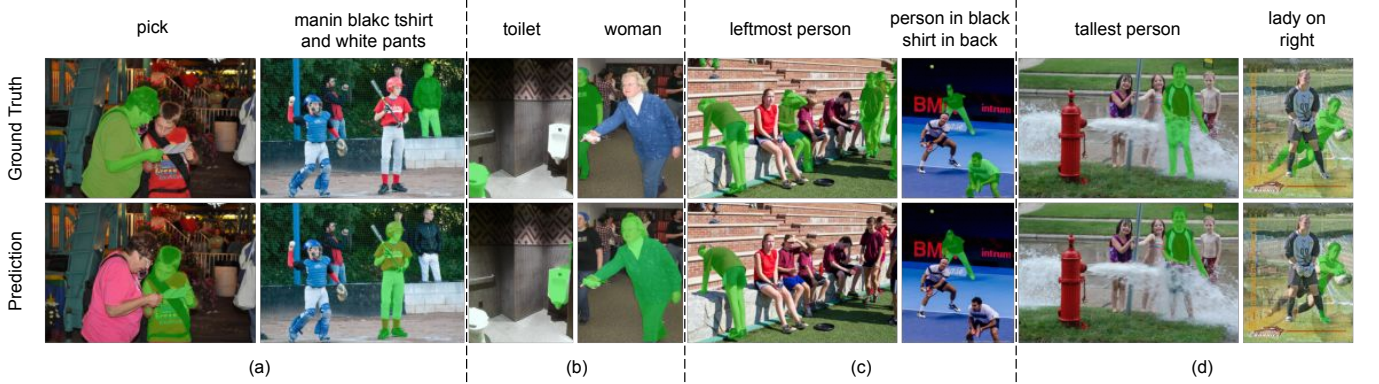


Fig. S1. Some incorrect predictions of our model on the UNC validation set. Each group (a-d) shows one pattern we observed within the predictions. The first row shows the ground truth mask, the second one is the prediction of our model.



Fig. S2. Colorization manipulation performance of different models on COCO validation examples.